Synaptic excitation of individual rat cerebellar granule cells *in situ*: evidence for the role of NMDA receptors

Egidio D'Angelo, Giovanna De Filippi, Paola Rossi and Vanni Taglietti

Istituto di Fisiologia Generale, Via Forlanini 6, I-27100, Pavia, Italy

1. Current-clamp recordings were made in whole-cell patch-clamp configuration from ninety-one granule cells in parasagittal cerebellar slices obtained from 21- to 31-day-old rats. Recordings were performed at 30 °C.

2. Resting membrane potential was -58 ± 6 mV ($n = 43$). The membrane voltage response to step current injection showed inward rectification consistent with increasing input resistance during membrane depolarization. Over -35 ± 7 mV ($n = 14$) repetitive firing with little or no adaptation was activated. Spike frequency increased nearly linearly with injected current.

3. Unitary EPSPs obtained by stimulating the mossy fibre bundle had an amplitude of $11{\cdot}4 \pm 2{\cdot}1$ mV ($n = 22$, holding potential $= -75$ mV). Synchronous activation of greater than one to two mossy fibres was needed to elicit action potentials. Antidromic stimulation elicited antidromic spikes and also EPSPs, presumably through a mossy fibre 'axon reflex'.

4. EPSPs were brought about by NMDA and non-NMDA receptor activation, accounting for about 70 and 30%, respectively, of peak amplitude at the holding potential of −70 mV. The EPSP decay conformed to passive membrane discharge after blocking the NMDA receptors.

5. No appreciable correlation was found between the time-to-peak and decay time constant of the EPSPs, consistent with the compact electrotonic structure of these neurons.

6. During membrane depolarization EPSP amplitude increased transiently, due to both a voltage-dependent increase of the NMDA component and inward rectification. In addition, EPSPs slowed down due to a slowdown of the NMDA component.

7. Temporal summation during high-frequency stimulation was sustained by NMDA receptors, whose contribution to depolarization tended to prevail over that of non-NMDA receptors during the trains. A block of the NMDA receptors resulted in reduced depolarization and output spike frequency.

8. This study, as well as extending previous knowledge to the intracellular level *in vivo*, provides evidence for a primary role of NMDA receptors in determining mossy fibre excitation of granule cells. It is suggested that the marked voltage dependence of the EPSP time course, which was mainly caused by voltage dependence in NMDA conductance, promotes the NMDA receptor-dependent enhancement of granule cell coding observed during repetitive mossy fibre activity.

Information entering the cerebellar cortex through the mossy fibre pathway is processed by granule cells before being relayed to Purkinje cells. The granule cell receives a single mossy fibre input on each of its three to five dendrites. Early studies using extracellular field recordings *in vivo* from the cerebellum of different species showed the excitatory nature of the mossy fibre–granule cell synapse and its inhibition by Golgi cells, as comprehensively reported by Eccles, Ito & Szentagothai (1967) and Ito (1984). Recently, patch-clamp whole-cell recordings from granule cells in cerebellar slices (D'Angelo, Rossi & Garthwaite, 1990; Silver, Traynelis & Cull-Candy, 1992; D'Angelo, Rossi & Taglietti, 1993) showed dual component excitatory postsynaptic currents (EPSCs), which were brought about by the activation of glutamate receptors of the *N*-methyl-D-aspartate (NMDA) and non-NMDA type.

It is generally assumed that non-NMDA receptors play a major role in determining excitatory postsynaptic potentials (EPSPs) during low-frequency stimulation,

while NMDA receptor activation occurs during high-frequency stimulation (Collingridge, Herron & Lester, 1988*b*; Collingridge, 1992). The role of NMDA receptors in synaptic transmission at low-frequency stimulation is controversial, depending on the neuron type and whether synaptic inhibition and extracellular Mg^{2+} are present (Collingridge, Herron & Lester, 1988*a*; Sutor & Hablitz, 1989; Lambert & Jones, 1990; Collingridge, 1992). In cerebellar granule cells, NMDA receptor involvement is expected to be particularly marked, since NMDA currents slow down considerably during membrane depolarization (D'Angelo, Rossi & Taglietti, 1994*b*), which may contribute to determining EPSP summation and neuronal firing during repetitive mossy fibre activity. Nevertheless, membrane potential changes induced by synaptic currents as well as the firing pattern of granule cells are still unknown, mainly because the tiny size of these neurons has, to date, precluded the use of conventional microelectrode techniques. In this study, we performed current-clamp recordings of granule cell activity in rat cerebellar slices using the whole-cell configuration of patch-clamp. We found that the NMDA conductance, owing to its complex voltage dependence, played a main role in determining both EPSP amplitude and time course at low frequency and EPSP summation and output spike frequency during repetitive mossy fibre activity.

METHODS

Whole-cell patch-clamp recordings were made from granule cells in the internal granular layer of rat cerebellar slices. Cerebellar slices were obtained from 21- to 31-day-old Wistar rats (day of birth = 1). Rats were anaesthetized with halothane (Aldrich) and killed by decapitation. The cerebellar vermis was isolated, glued to the stage of a vibroslicer (Campden Instruments, London) and rapidly immersed in oxygenated Krebs solution at 10 °C. Slices, 200–300 μm thick, were cut in the parasagittal plane and maintained at room temperature (19–21 °C) in oxygenated Krebs slolution for at least 30 min before being transferred to the recording chamber (D'Angelo *et al.* 1990, 1993).

Recording and analysis

Patch pipettes were pulled from thick-walled borosilicate glass capillaries (Hingelberg, Malsfeld, Germany) and had 8–12 MΩ resistance before seal formation. Electrical stimulation of afferent fibres was performed with a bipolar tungsten electrode (Clark Instruments, Pangbourne, UK) via a stimulus insulation unit. In some experiments, a second stimulating electrode was located at the edge of the molecular layer. Stimulating pulses lasting 100–200 μs were usually delivered at 0·25 Hz. Pulse trains of variable frequency and duration were set using a Digitimer D100 logical unit.

Tight-seal whole-cell recordings were performed conventionally (Edwards, Konnerth, Sakmann & Takahashi, 1989) using the 'blind patch' approach. Membrane current and voltage were recorded using an Axopatch-1D patch-clamp amplifier (Axon Instruments; output cut-off frequency = 10 kHz). Signals were simultaneously stored on a DAT recorder (Biologic DTR-1201; Biologic, Claix, France) and fed to the mass memory of a PC (sampling frequency = 250 μs for current-clamp recordings, 10–50 μs for voltage-clamp recordings). Acquisition and data analysis were done using pCLAMP (Axon Instruments) and SCAN (kindly provided by Dr John Dempster) software. Data were reported as means ± S.D. and the number of observations is indicated in parentheses. Statistical comparisons were done using Student's t test.

Analysis of current transients activated by 10–20 mV hyperpolarizing steps from the holding potential of −70 mV in voltage-clamp mode (Silver *et al.* 1992; D'Angelo *et al.* 1993) gave the following values ($n = 79$ for all measures): membrane input resistance $R_m = 2{\cdot}3 \pm 1{\cdot}1$ GΩ, membrane input capacitance $C_m = 3{\cdot}1 \pm 1{\cdot}5$ pF, membrane time constant $\tau_m = R_m C_m = 6{\cdot}7 \pm 3{\cdot}3$ ms, decay time constant of the current transient $\tau_s = 57{\cdot}9 \pm 24$ μs, series resistance $R_s = \tau_s / C_m = 18{\cdot}5 \pm 15{\cdot}6$ MΩ.

In current-clamp mode, electrode capacitance compensation was critical in recording membrane voltage changes reliably (Fig. 1), since granule cell membrane capacitance (3 pF) was comparable to electrode capacitance (5 pF). Electrode capacitance was compensated electronically using the value matched during current transient cancellation in cell-attached configuration. Cancellation achieved by maintaining the immersion depth to 1 mm or less and holding the electrode at a rather steep angle (45–60 deg) was virtually complete and no effective improvement was obtained after having reduced the electrode capacitive current with Sylgard coating. The current charging the patch-pipette was provided by the feed-back 'negative capacitance' compensation circuit in the Axopatch-1D amplifier (Fig. 1). Note that capacitive compensation currents, due to their dependence on the rate of membrane potential change, are much greater during action potentials than during the EPSPs. Nearly maximal compensation was usually achieved, since <10% overcompensation invariably produced oscillations. On the other hand, decreasing negative capacitance compensation slowed membrane charging considerably.

Error estimates in voltage measurements

Pipette offset was compensated electronically. Since liquid junction potential was <2 mV, membrane potential values were left uncorrected. Field potentials produced by neighbouring granule cell activity, which were measured after removing the pipette from the cell and cleaning its tip by gently applying positive pressure, were smaller than 0·5 mV ($n = 8$) and therefore did not appreciably modify the transmembrane potential.

Attenuation of a constant command potential across the electrode resistance ($R_e = 10$ MΩ) was calculated by considering current partitioning between the seal leak resistance ($R_l > 20$ GΩ) and cell input resistance (either $R_m = 0{\cdot}5$ GΩ or $R_m = 5$ GΩ to simulate inward rectification), according to the equation $V_p / V_c = 1 - [R_e(R_m + R_l)/R_m R_l]$. Attenuation of V_p caused by the voltage drop across the access resistance ($R_a = R_s - R_e = 10$ MΩ) was obtained as $V_m / V_p = 1 - [R_a / R_m]$. With the resistance values given, the membrane potential ratio V_m / V_c was >0·94 for $R_m = 0{\cdot}5$ GΩ and >0·996 for $R_m = 5$ GΩ. Consistent with negligible voltage attenuation, bridge compensation did not produce any appreciable changes in EPSPs or passive voltage transients ($n = 11$, not shown).

Attenuation of a potential generated by mossy fibre synapses at the end of the dendrites and measured from the soma was estimated using a neuron model consisting of a spherical soma

(diameter = 6 μm) connected to four identical unbranched dendrites (diameter = 1 μm, length = 10 μm) and an axon (diameter = 0·1 μm). The procedure used is based on cable's equations and is formally similar to that reported by Mugnaini, Atluri & Houk (1974). Computations were carried out using a specific axoplasmic resistance of 80 Ω cm and a specific membrane resistance of either 1500 Ω cm^2 or 15000 Ω cm^2 to simulate inward rectification. In the absence of synaptic inputs, soma-to-dendritic membrane potential ratios were 0·981 and 0·998, respectively. When an active load of 500 pS (which is a reasonable estimate of synaptic conductance; D'Angelo *et al.* 1993) was applied to one to four dendrites, calculations yielded soma-to-dendritic membrane potential ratios of 0·977, 0·972, 0·967 and 0·962, respectively (R_m = 0·5 GΩ), and 0·993, 0·988, 0·983 and 0·978, respectively (R_m = 5 GΩ). Therefore, in current-clamp as well as in voltage-clamp conditions (Silver *et al.* 1992; D'Angelo *et al.* 1993), the granule cells tend to behave like a single electrical compartment.

Solutions and drugs

Krebs solution for slice cutting and recovery contained (mM): NaCl, 120; KCl, 2; $MgSO_4.7H_2O$, 1·2; $NaHCO_3$, 26; KH_2PO_4, 1·2; $CaCl_2$, 2; glucose, 11. This solution was equilibrated with 95% O_2 and 5% CO_2 (pH 7·4) and was perfused at a rate of 2–4 ml min^{-1}. The recording chamber had a volume of 1·5 ml and was maintained at 30 ± 1 °C.

The intracellular solution contained (mM): potassium gluconate, 122; KCl, 4; NaCl, 4; $MgCl_2$, 1; $CaCl_2$, 0·02; BAPTA, 0·1; glucose, 15; ATP, 3; Hepes, 5; pH was adjusted to 7·2 with KOH. This solution buffered intracellular Ca^{2+} at 100 nM.

D-2-amino-5-phosphonovaleric acid (APV), 6-cyano-7-nitroquinoxaline-2,3-dione (CNQX) and 7-chlorokinurenic acid (7-Cl-Kyn) were obtained from Tocris Neuramin (Bristol, UK). Glycine, bicuculline and tetrodotoxin (TTX) were obtained from Sigma. The synthetic peptide ω-conotoxin (ω-CgTx) was obtained from Peninsula Laboratories (Belmont, CA, USA) and BAPTA tetrapotassium salt from Molecular Probes (Eugene, OR, USA).

Drugs dissolved in extracellular Krebs solution were applied locally through a multi-barrelled pipette. Unless stated otherwise, all solutions perfused during recordings contained 10 μM glycine and 10 μM bicuculline.

RESULTS

Whole-cell patch-clamp recordings were performed in ninety-one granule cells in cerebellar slices obtained from 21- to 31-day-old rats. In order to investigate the excitatory action of mossy fibres in isolation, all the experiments were performed with 10 μM bicuculline in recording solutions to block inhibitory synapses. In preliminary experiments EPSPs did not change significantly when a nominally glycine-free medium was exchanged with a medium containing 10 μM glycine. Amplitude was +0·6 ± 2·8% and half-width (HW), −2·1 ± 2·8% of control (n = 6), suggesting that endogenous glycine saturated the NMDA receptor glycine-binding site (Mayer, Vyklicky & Clements, 1989;

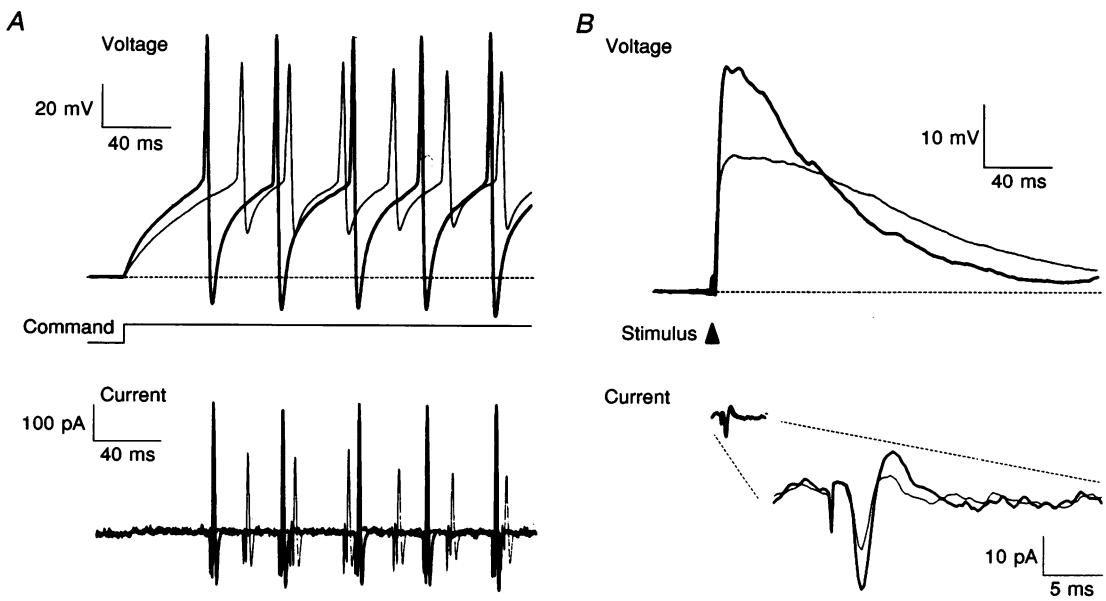

Figure 1. Effect of electrode capacitance compensation on action potentials (*A*) and EPSPs (*B*) recorded from cerebellar granule cells in whole-cell patch-clamp configuration (current-clamp mode)

Voltage recordings are shown at the top together with the corresponding current command (a 7 pA step) and the mossy fibre stimulus (arrowhead). Both action potentials and EPSPs are elicited from the membrane potential of −70 mV. The corresponding currents generated by the amplifier, consisting of the sum of command and capacitive compensation currents, are shown at the bottom (note the different scales in *A* and *B*). Thick traces were recorded at the best of electrode capacitance compensation and thin traces after reducing compensation by 50%. Stimulus artifacts have been partially blanked.

Thomson, 1989). Subsequent experiments have been carried out with 10 μM glycine in recording solutions.

Current-clamp recordings required careful compensation of electrode capacitance (see Methods). In these conditions membrane charging speeded up and the current-clamp system allowed 60–90 mV spikes (measured from threshold to the peak of the upstroke) with HW = 1·5 ms to be resolved, in a similar way to many other neurons recorded with conventional microelectrode techniques (Fig. 1*A*). The rate of membrane potential change, measured as the first derivative of action potentials ($n = 10$), reached values that were usually greater than 50 V s^{-1}. As well as action potentials, EPSPs were also remarkably increased in amplitude and their time course was speeded up by compensating electrode capacitance (Fig. 1*B*).

Passive membrane properties of rat cerebellar granule cells

No spontaneous extracellular action currents were observed during seal formation, nor was any spontaneous firing seen after patch disruption. Granule cell resting membrane potential measured soon after gaining access to the cell was −57·8 ± 6·4 mV ($n = 43$; range from −45 to −72 mV).

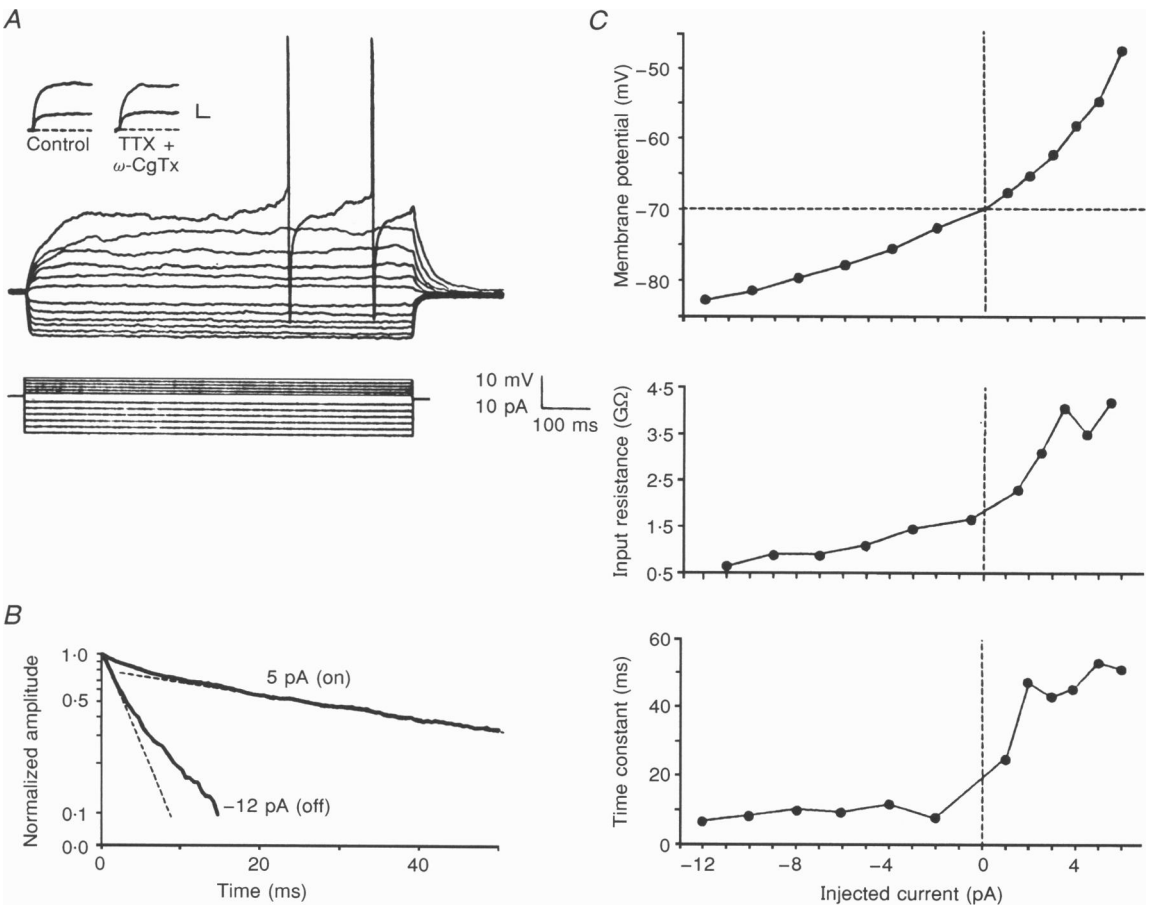

Figure 2. Passive properties of cerebellar granule cells

Data in the figure (except the insets to panel *A*) are obtained from the same cell (holding potential = −70 mV). *A*, voltage transients obtained in response to current steps applied through the patch electrode (1 pA in the depolarizing direction, 2 pA in the hyperpolarizing direction). Two action potentials are activated in the uppermost trace. Insets show subthreshold depolarizations elicited by 4 and 8 pA current steps from the holding potential of −80 mV in control and after 5 μM ω-CgTx + 0·5 μM TTX application (scale bars 10 mV, 100 ms). *B*, semilogarithmic plots (thick lines) of the on-response to a 5 pA current pulse and of the off-response to a −12 pA current pulse. Voltage transients are normalized to unitary amplitude and are made to decay to zero. Dashed lines demonstrate divergence from linearity of membrane charging kinetics. *C*, voltage transient parameters as a function of injected current. The voltage–current plot (top) shows membrane potential attained at steady state. Input resistance (middle) is the slope of the voltage–current plot measured between neighbouring points. Membrane time constant (bottom) is the slope of lines fitted to semilogarithmic plots of voltage transients, as indicated in *B*.

Granule cell membrane properties were investigated by setting the membrane potential ('holding potential') at −70 mV with constant current injection. As shown in Fig. 2*A*, voltage transients were induced with step current injection in both the depolarizing and hyperpolarizing directions. Voltage transients relaxed monotonically towards a steady-state level whose amplitude was non-linearly related to the current applied, resulting in strong inward rectification in voltage–current plots (Fig. 2*C*, top panel). Apparent input resistance (R_m) was calculated as the slope of the voltage–current plot (Fig. 2*C*, middle panel).

Membrane charging was slower in the depolarizing than in the hyperpolarizing transients, suggesting that R_m, and hence $\tau_m = R_m C_m$, was greater in the former than in the latter. Using semilogarithmic plots of the voltage transients, we noted that charging rate decreased with time (Fig. 2*B*), consistent with the increase of R_m along with development of membrane depolarization. Since the slope of voltage transients varied with time, in order to estimate τ_m we measured the slope of regression lines fitted to the late portion of the on-response in depolarizing transients and to the initial portion of the off-response in hyperpolarizing transients (Fig. 2*B*). Indeed, these τ_m values (Fig. 2*C*, lower panel) paralleled those of membrane input resistance measured at steady state, consistent with a real increase of input resistance during membrane depolarization (Wilson, 1992). Inward rectification was similar before and after 5 μM ω-CgTx + 0·5 μM TTX application ($n = 3$, Fig. 2*A*, inset), indicating that neither Ca^{2+} currents – whose mature form in granule cells is blocked by over 90% by ω-CgTx (Rossi, D'Angelo, Magistretti, Toselli & Taglietti, 1994) – nor TTX-sensitive Na^+ currents contributed noticeably to subthreshold membrane depolarization.

On average, R_m was 0·6 ± 0·4 and 5·1 ± 2·5 GΩ at −88 and −55 mV, respectively, and τ_m was 5·9 ± 2·4 and 42·7 ± 10·9 ms at −88 and −55 mV, respectively ($n = 17$ for all values). R_m therefore increased by 9 times and τ_m increased by 7 times, from −88 to −55 mV. It should be noted that τ_m relative to −88 mV was not significantly different from τ_m measured in voltage-clamp conditions (5·1 ± 1·4 ms, $n = 17$; $P < 0·01$), confirming that electrode capacitance compensation was adequate (cf. Fig. 1 and Methods for details).

Action potentials activated by current injection

Upon injection of depolarizing current pulses, at a threshold of −35 ± 7 mV ($n = 14$; threshold was measured at the first point of the upstroke), granule cells produced action potentials (Fig. 2*A*). Action potentials consisted of a small prepotential followed by the upstroke (HW = 1·4 ± 0·3 ms, $n = 14$). The upstroke overshot to 31 ± 10 mV and was followed by rapid hyperpolarization to −82 ± 17 mV ($n = 14$). Activation of the first spike was often delayed by a small downward deflection observed in voltage transients near the threshold (Fig. 2*A*), presumably in relation to activation of the fast-inactivating K^+ current (I_A) reported in rat cerebellar granule cells (Cull-Candy, Marshall & Ogden, 1989; Bardoni & Belluzzi, 1993).

Spikes occurred in regular trains (Fig. 3*A*, top) showing little or no adaptation during 800 ms current steps (Fig. 3*A*, bottom). Spike frequency increased with the

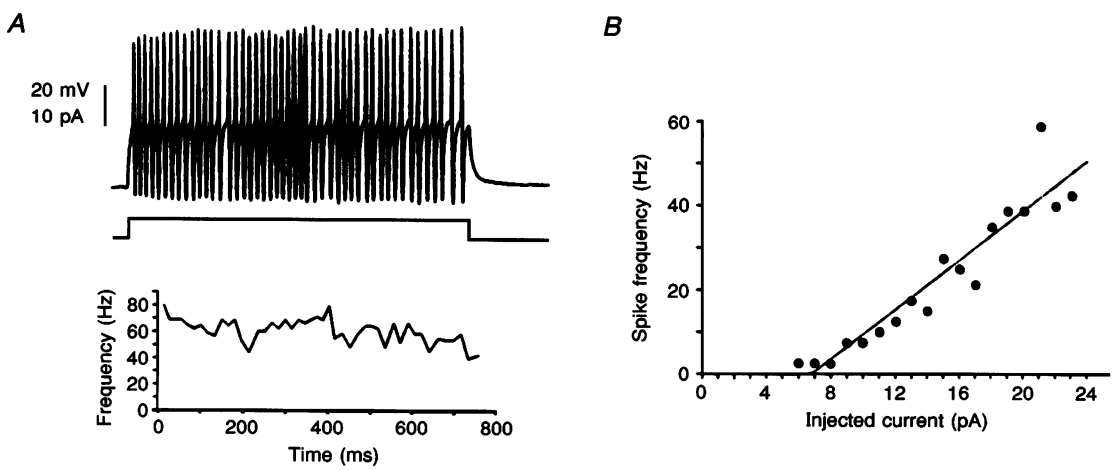

Figure 3. Firing of action potentials in a granule cell

Data from the same cell shown in Fig. 2 (holding potential = −70 mV). *A*, repetitive response (top) during injection of a 21 pA current pulse (middle). The diagram at the bottom reports the instantaneous action potential frequency calculated as the inverse of the interspike interval. *B*, spike frequency averaged over the whole current pulse duration (800 ms) plotted as a function of injected current. The line fitted to the points had slope of 2·94 spikes (s pA)$^{-1}$ and *x*-axis intercept at 6·8 pA ($r = 0·92$).

intensity of injected current (Fig. 3*B*). The average spike frequency measured over the entire current pulse was used to construct current–frequency plots, which could be fitted to a straight line ($r > 0{\cdot}9$) with slopes ranging from 2 to 11 spikes (s pA)$^{-1}$ (mean slope = $6{\cdot}5 \pm 3{\cdot}2$ spikes (s pA)$^{-1}$, x-axis intercept = $6{\cdot}1 \pm 3{\cdot}2$ pA, $n = 18$). Spikes were blocked by 0·5 μM TTX application (not shown).

Mossy fibre activation of granule cells

Electrical stimulation of the axial fibre bundle containing afferent mossy fibres activated synaptic depolarizing potentials (Fig. 4*A*). In these experiments, holding potential was maintained at between −60 and −80 mV. The delay to onset of the EPSPs was $1{\cdot}7 \pm 0{\cdot}4$ ms ($n = 25$), consistent with monosynaptic granule cell activation. At increasing stimulus intensities, EPSPs reached the threshold for action potential activation. Action potentials occurred usually as singlets, the time-to-peak (TTP) for the first spike being $4 \pm 1{\cdot}6$ ms ($n = 11$).

Small changes in stimulus intensity made the EPSP jump between amplitude levels (Fig. 4*A* and *B*), identification of which was usually facilitated by narrow amplitude variation within each level. Note in Fig. 4*B* that similar EPSP amplitude levels could be obtained at different experimental times, demonstrating the stability of recording and stimulation, and that occasional transitions occurred spontaneously between neighbouring levels maintaining the same stimulus intensity. Since each mossy fibre forms just one synapse with a cerebellar granule cell and each granule cell receives three to five mossy fibres (Ito, 1984), transitions between levels could be explained by activation of a different number of individual mossy fibre synapses. Accordingly, from holding potentials between −60 and −80 mV, we could usually distinguish between two and four EPSP amplitude levels indicating activation of two to four synapses and the existence of an additional synapse was signalled by activation of action potentials at higher stimulus intensities, yielding a maximum number of active synapses between three and five ($n = 35$, Table 1).

In three granule cells requiring activation of three synapses to activate an action potential, the presence of a fourth synapse was suggested by reduction of latency to the first spike and activation of a second/third spike following a further increase of stimulus intensity (not shown). From holding potentials between −50 and −60 mV, two synapses were often sufficient to activate action potentials, which occurred as sequences of two to three spikes.

Direct counting of active granule cell synapses provided two main clues: (1) action potentials were obtained after synchronous activation of at least two to three synapses over a rather wide range of membrane potentials; (2) the unitary EPSP amplitude could be measured directly, proving to be $11{\cdot}4 \pm 2{\cdot}1$ mV from the holding potential of -75 ± 5 mV ($n = 22$). EPSPs generated by a second and third synapse summed nearly linearly, in spite of the considerable reduction in driving force and were broader than unitary EPSPs (Table 1, see also Fig. 4*A* and *B*), due to EPSP voltage dependence (see Fig. 7 and Discussion).

Antidromic stimulation of granule cells

At intensities usually higher than those required for stimulation of the mossy fibre bundle, antidromic spikes were activated in seven out of thirteen cells tested by electrical stimulation at the edge of the molecular layer (Fig. 4*C*). The delay to spike upstroke was $2 \pm 0{\cdot}9$ ms ($n = 7$), accounting for a mean apparent axonal conduction velocity of 0·2 m s^{-1} to cover approximately 400 μm between the stimulating and recording electrodes. Inability to record antidromic spikes in many of the cells tested was probably due to the interruption of ascending axons or parallel fibres travelling orthogonally to the slice.

In addition to activating antidromic spikes, in eight cells stimulation at the edge of the molecular layer elicited EPSPs similar to those obtained with stimulation of the mossy fibre bundle (Fig. 4*D*), albeit after a longer delay (2–4 ms). The longer delay suggested that these EPSPs were likely to have been activated by antidromic invasion of mossy fibre collaterals rather than by current spread to

Table 1. EPSP parameters during mossy fibre recruitment

No. of MFs	EPSP amplitude (mV)	EPSP TTP (ms)	EPSP HW (ms)	No. of obs.	No. of GCs with AP
1	$11{\cdot}4 \pm 2{\cdot}1$	$8{\cdot}7 \pm 3{\cdot}4$	$31{\cdot}6 \pm 14{\cdot}6$	22	—
2	$25 \pm 5{\cdot}7$	6 ± 2	$31{\cdot}3 \pm 17{\cdot}5$	16	—
3	$29 \pm 1{\cdot}6$	$6{\cdot}8 \pm 2{\cdot}9$	$48{\cdot}4 \pm 26$	6	6
4	$38 \pm 0{\cdot}1$	$6{\cdot}1 \pm 2{\cdot}3$	$61{\cdot}1 \pm 24$	2	4
5	—	—	—	—	2

Amplitude, TTP and HW of EPSPs obtained by activating a different number of mossy fibre (MF) inputs. In some of these granule cells (GCs) activation of 3–5 mossy fibres activated an action potential (AP), as indicated in the rightmost column. Mean holding potential was -75 ± 5 mV ($n = 22$).

the mossy fibre bundle, since conduction along terminal mossy fibre branches was slower than along proximal branches (Eccles *et al.* 1967). Results obtained with orthodromic and antidromic stimulation were interpreted following the scheme shown in Fig. 4*E* (see also Discussion). All the experiments reported below were obtained by stimulation of the mossy fibre bundle.

EPSP pharmacology

Mossy fibre–granule cell synaptic transmission is brought about by activation of glutamate receptors of the NMDA and non-NMDA type (Garthwaite & Brodbelt, 1989; Silver *et al.* 1992; D'Angelo *et al.* 1993). We first considered EPSP pharmacology at the holding potential of −70 mV.

As shown in Fig. 5*A*, application of 20 μM CNQX, which is quite selective for non-NMDA receptors with 10 μM glycine, considerably reduced the EPSPs. In these experiments, control EPSP amplitude was 16·3 ± 3·2 mV ($n = 7$) and was reduced by 85 ± 9% after CNQX application. The remaining NMDA EPSP was then nearly abolished by 50–100 μM APV. Direct application of either 50–100 μM APV (Fig. 5*B*), an antagonist of the glutamate-binding site, or of 50 μM 7-Cl-Kyn (not shown), an antagonist of the NMDA receptor glycine-

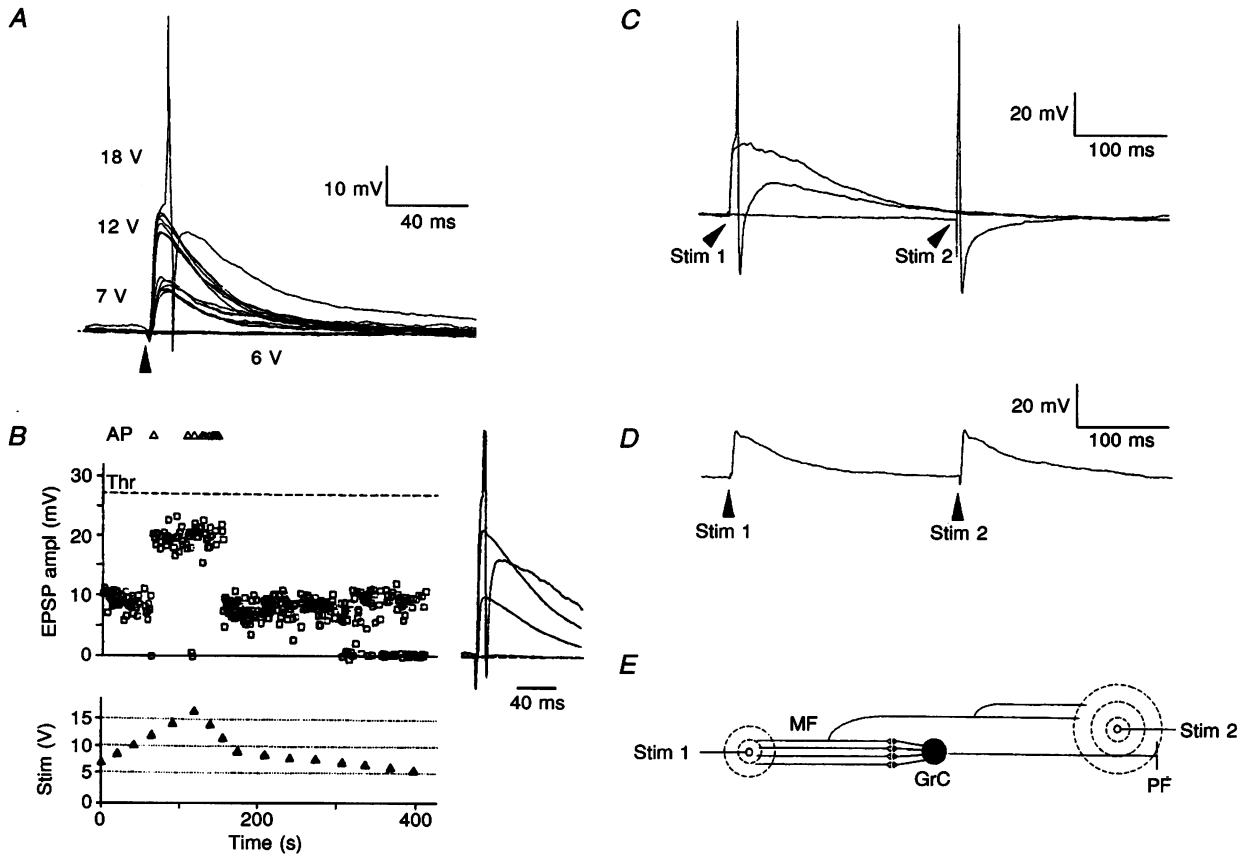

Figure 4. Mossy fibre stimulation and antidromic invasion of granule cells

A, superimposed traces obtained following mossy fibre stimulation (arrowhead, Stim 1) showing failures (6 V), EPSPs (7 V and 12 V) and EPSP-activated action potentials (18 V). Holding potential = −70 mV. *B*, EPSPs were recorded while changing stimulus intensity in small steps, as represented schematically at the bottom. EPSP amplitude stepped over two different levels following small stimulus changes, until it crossed the amplitude threshold (Thr) for action potential activation (AP). Insets to the right (same amplitude scale as in the plot) are averages of 20 individual traces at the failure, first and second EPSP amplitude level and a single EPSP with action potential (truncated). *C*, stimulation of the mossy fibre bundle (Stim 1, 8 V) gave EPSPs and EPSP-activated action potentials similar to those in *A* and *B*. An antidromic action potential was elicited by stimulation of the molecular layer by a different electrode (Stim 2, 15 V). *D*, stimulation of either the mossy fibre bundle (Stim 1, 7 V) or the molecular layer (Stim 2, 16 V) evoked similar EPSPs. Delay to onset of the EPSPs evoked by Stim 1 and Stim 2 were 1·6 ms and 3 ms, respectively. *E*, schematic drawing illustrating cerebellar granule cell wiring and the presumed pathways activated in the present experiments. Stim 1 and Stim 2, stimulating electrodes, GrC, cerebellar granule cell; MF, mossy fibres; PF, parallel fibres. Dashed lines indicate potential fields of stimulating electrodes.

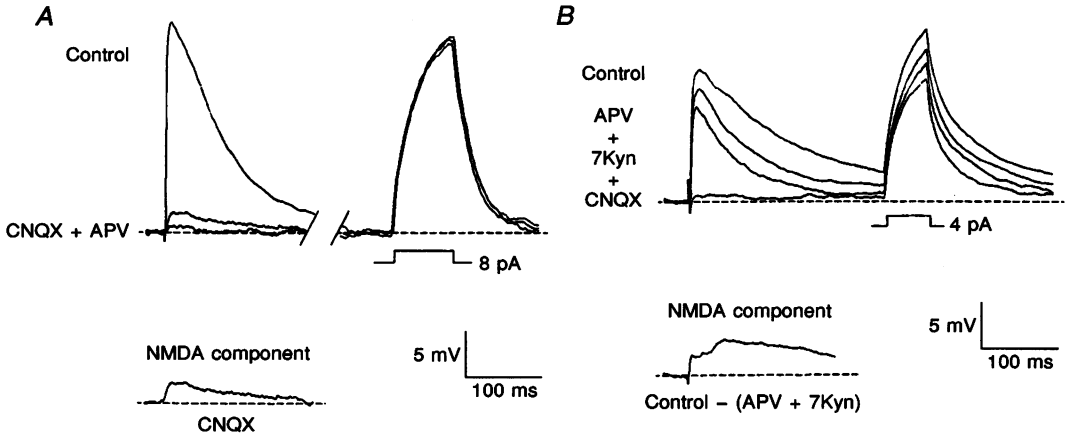

Figure 5. EPSP pharmacology

EPSPs are followed by a voltage transient activated by step current injection (averages of 8–12 traces, holding potential = −70 mV). In this and the following figures, '7Kyn' indicates 7-Cl-Kyn. *A*, effect of 20 μM CNQX application and of subsequent addition of 100 μM APV. The NMDA component (CNQX trace) is replotted at the bottom. *B*, additive effects of subsequent applications of 100 μM APV, 50 μM 7-Cl-Kyn and 20 μM CNQX. The NMDA EPSP-component was obtained by subtracting the APV + 7-Cl-Kyn trace from control (bottom). In this example passive transients are distorted by overlap with the EPSP tail.

binding site (Henderson, Johnson & Asher, 1990), reduced the amplitude and accelerated the decay phase of control EPSPs. It should be noted that application of 7-Cl-Kyn enhanced NMDA receptor block produced by APV (Fig. 5*B*) presumably because, as shown by quantitative autoradiography, inhibition by 100 μM APV of [^{3}H]glutamate–NMDA receptor binding in the presence of 10 μM glycine in the internal granular layer of the rat cerebellum is incomplete (Monaghan & Anderson, 1991).

In the present experiments, control EPSP amplitude, TTP and HW were 14·4 ± 2·1 mV, 10·8 ± 2·8 ms and 49·3 ± 21·2 ms, respectively ($n = 9$). After NMDA receptor block, amplitude, TTP and HW were reduced by 29, 22 and 13%, respectively. The remaining non-NMDA EPSP was readily blocked by CNQX at 10–20 μM (Fig. 5*B*), indicating that APV and 7-Cl-Kyn co-application produced a nearly complete block of the NMDA-receptors.

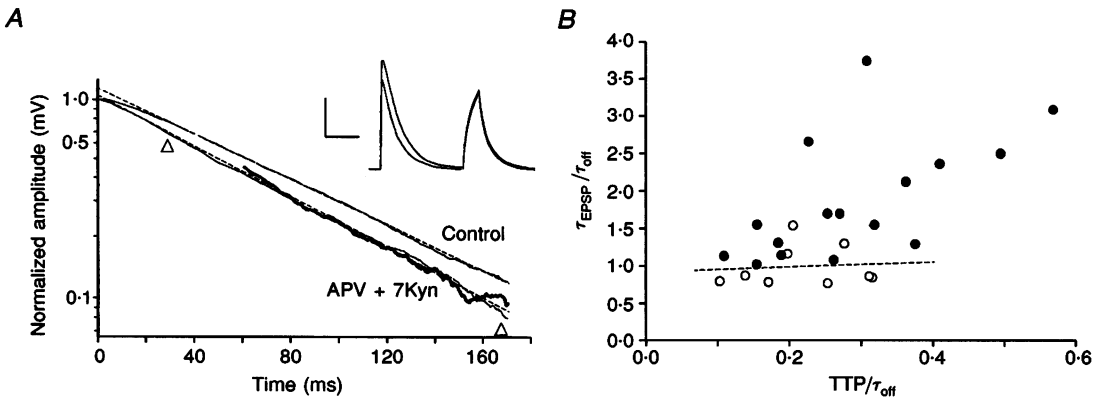

Figure 6. Time course of EPSPs in control conditions and after NMDA receptor block by 100 μM APV + 50 μM 7-Cl-Kyn

A, semilogarithmic plots of EPSP decay. Straight lines (dashed) were fitted to EPSP decay ($r > 0·99$), the time constants being 55 ms in control and 43·4 ms in non-NMDA EPSPs (triangles indicate limits for fitting). The decay time constant of a passive transient (thick line shown superimposed on the non-NMDA EPSP decay) was 46·3 ms. Experimental traces are shown in the inset (holding potential = −70 mV; calibration bars 10 mV, 100 ms). *B*, scatter plot of τ_{EPSP} *vs.* TTP normalized by the membrane time constant measured from passive transients (τ_{off}). Data points correspond to different granule cells. ●, control EPSPs; ○, non-NMDA EPSPs. The dashed line shows linear regression to the non-NMDA EPSP points. Holding potential = −70 mV.

A comparison of the lower traces in Fig. 5*A* and *B* shows that the NMDA component obtained by subtracting non-NMDA from control EPSP was greater than that obtained by CNQX application, average reductions relative to control peak amplitude (29 and 15%, respectively) being significantly different ($P < 0{\cdot}01$). The greater size of the NMDA component obtained with the subtraction procedure than after CNQX application was probably due to enhanced removal of Mg^{2+} block from the NMDA channels (Asher & Nowak, 1988), since membrane depolarization is greater in the former case than in the latter.

Passive membrane properties did not change during drug application, as indicated by the constancy of voltage transients activated by step current injection (Fig. 5*A* and *B*).

The factors controlling the EPSP time course

The influence of the NMDA component on EPSP decay was investigated by comparing the EPSP decay time constant (τ_{EPSP}) with the membrane time constant estimated from decay of voltage transients of comparable size (τ_{off}). This analysis is exemplified with recordings obtained from the holding potential of −70 mV, while the voltage-dependent action of the NMDA component on EPSP time course is considered in the next chapter. As shown in Fig. 6*A*, EPSP and voltage transient decays were normalized to unitary amplitude and plotted on a semilogarithmic scale. Linear fittings to the plots were

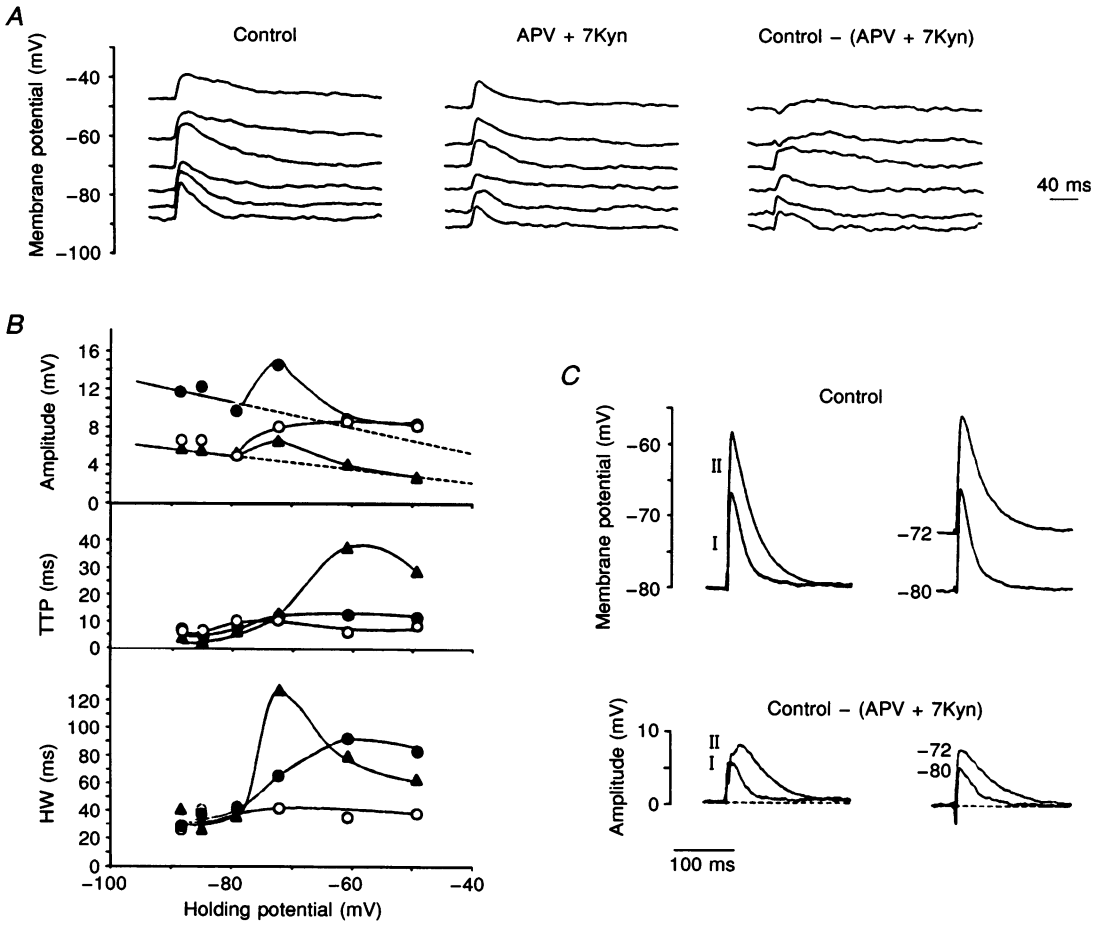

Figure 7. Voltage dependence of the EPSPs

A, EPSPs (average of 4 traces) were recorded from different holding potentials in control solution (left) and after 100 μM APV + 50 μM 7-Cl-Kyn application (middle). NMDA EPSPs (right) are the difference between control and non-NMDA traces. *B*, peak amplitude, TTP and HW are plotted *vs.* the holding membrane potential for the EPSPs shown in *A*. ●, control EPSPs; ○, non-NMDA EPSPs; △, NMDA EPSPs. Continuous lines have been drawn through the points and, in amplitude, plots their straight portion has been extended towards 0 mV on the *x*-axis (dashed lines). *C*, average EPSPs were obtained from 12 traces recorded either from the same holding potential (−80 mV) but at two different stimulus intensities (I and II, upper left), or from two different holding potentials (−80 and −72 mV, upper right) at the same stimulus intensity. NMDA EPSPs obtained by subtracting non-NMDA traces (obtained by applying 100 μM APV + 50 μM 7-Cl-Kyn, not shown) from control traces are shown at the bottom.

then performed by excluding the initial non-linear portion of the curves ($r > 0{\cdot}98$). The following values were obtained ($n = 9$ for all values): τ_{EPSP} (control) $= 74 \pm 33{\cdot}8$, τ_{EPSP} (non-NMDA) $= 48{\cdot}6 \pm 17{\cdot}1$, $\tau_{off} = 46{\cdot}7 \pm 15{\cdot}4$. τ_{EPSP} (non-NMDA) was not significantly different from τ_{off} ($P < 0{\cdot}001$), while τ_{EPSP} (control) was significantly greater than the two other constants ($P < 0{\cdot}02$). The NMDA component therefore significantly slowed down the EPSP decay phase, which conformed to passive charge distribution on the cell membrane after NMDA receptor block (Forsythe & Westbrook, 1988).

The EPSP time course was compared between different granule cells by plotting τ_{EPSP} *vs.* TTP values normalized by τ_{off} (Fig. 6*B*). In these plots variability related to passive membrane properties (R_m and C_m) was therefore suppressed. Residual variability of τ_{EPSP}/TTP values in control EPSPs (filled circles) was much reduced by NMDA receptor block (open circles). This result may be explained if one considers that, as the EPSP time course is controlled by the NMDA conductance, it reflects the intrinsic variability in the NMDA conductance and/or voltage dependence (D'Angelo *et al.* 1993, 1994*b*). On the other hand, the time course of non-NMDA EPSPs, which conforms to passive membrane charging, was very similar in different granule cells.

The τ_{EPSP}/TTP shape index has often been used to investigate EPSP transmission from synapses to the recording site (Spruston, Jaffe & Johnston, 1994). In the non-NMDA EPSPs (Fig. 6*B*), no significant τ_{EPSP}/TTP correlation was found ($r = 0{\cdot}01$), suggesting either that

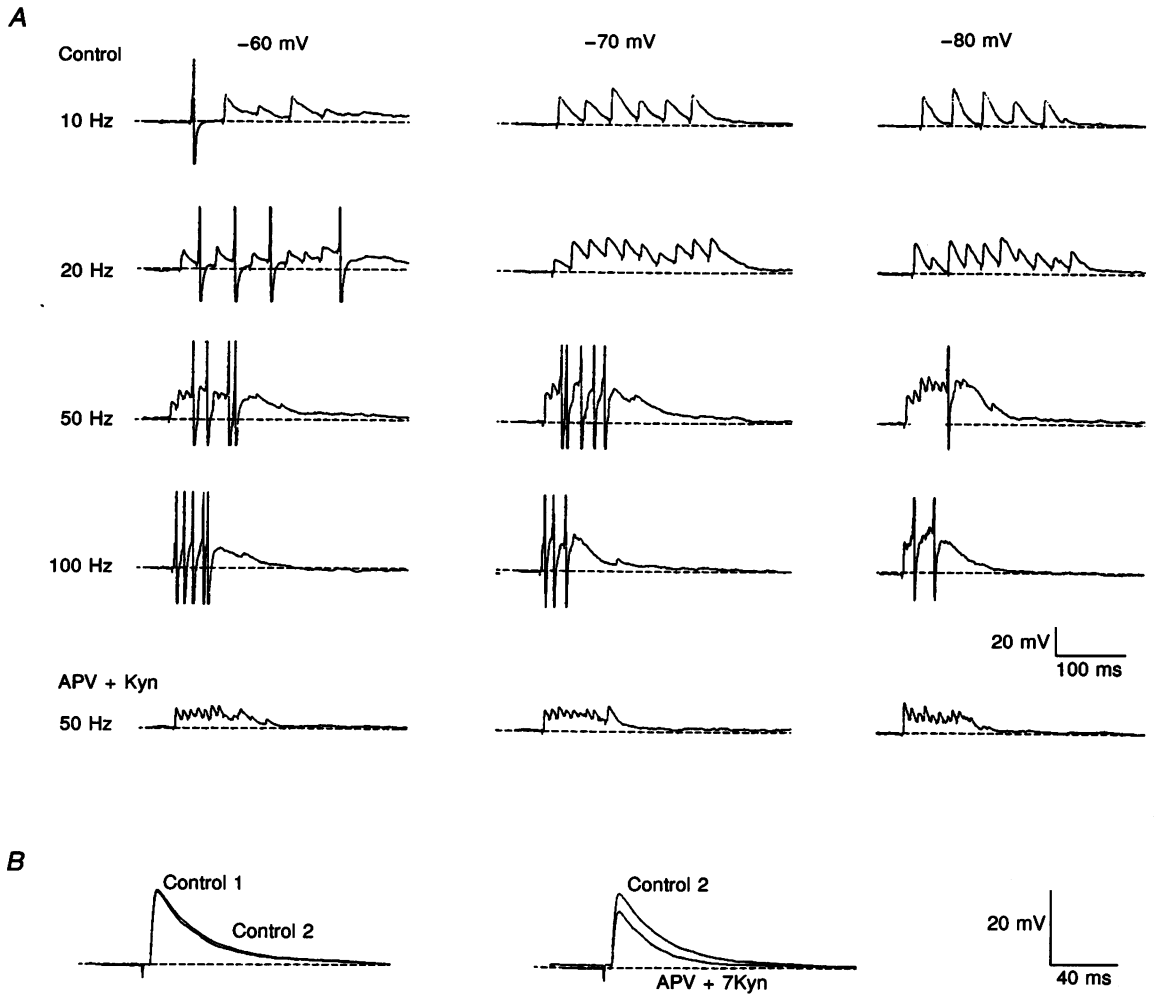

Figure 8. Repetitive stimulation of granule cells

A, stimulus trains were delivered at 10, 20, 50 and 100 Hz and granule cell activity was recorded at −60, −70 and −80 mV. EPSP summation eventually led to action potential firing (spikes are truncated). Application of 100 μM APV + 50 μM 7-Cl-Kyn reduced EPSP summation and the probability of action potential firing, as illustrated for the 50 Hz trains. *B*, EPSPs measured after the control stimulus trains (Control 2) recovered to their original size (Control 1). Thereafter, NMDA receptors were blocked by 100 μM APV + 50 μM 7-Cl-Kyn application. Same cell as in *A*.

EPSP electrotonic distortion was quite similar in different granule cells, or that distortion was negligible. Negligible electrotonic distortion is indeed supported by simulation of potential diffusion in granule cell dendrites (see Methods), since potential attenuation from synapses to soma is $<2\%$ even when input conductance is increased during synaptic activity.

EPSP voltage dependence: role of the NMDA component

EPSPs showed complex voltage dependence in their amplitude and time course (Fig. 7*A*). EPSPs became broader the more depolarized the holding membrane potential and increased transiently in amplitude from holding potentials around −70 mV (left traces). This voltage dependence was reduced in non-NMDA EPSPs (middle traces), as it may be better appreciated by comparing the uppermost with lowermost traces. Consistent with previous voltage-clamp analysis of the NMDA EPSCs (D'Angelo *et al.* 1994*b*), the NMDA EPSP rising and decaying phase slowed down at depolarized membrane potentials (right traces).

In Fig. 7*B*, the voltage dependences of peak amplitude, TTP and HW were compared in controls (filled circles), non-NMDA (open circles) and NMDA EPSPs (triangles). The NMDA component showed an evident increase and slowdown at holding potentials positive to −80 mV, contributing substantially to increasing EPSP peak amplitude and prolonging EPSP TTP and HW. The non-NMDA component also increased considerably due to inward rectification (cf. Fig. 2), but showed only modest HW and TTP prolongation. It should be noted that, at increasing membrane depolarization, NMDA's contribution to EPSP peak amplitude tended to vanish, since the NMDA EPSP peaked later than the non-NMDA EPSP, so that EPSP amplitude reflected quite closely the amplitude of the non-NMDA EPSP. The voltage dependence of the NMDA and non-NMDA components explained the transient amplitude increase in the EPSPs at holding potentials around −70 mV, as shown in Fig. 7*B* by the divergence of EPSP amplitude from reference lines passing through the ideal 0 mV reversal potential of the receptors. Similar results were observed in five other cells (mean TTP was $6{\cdot}5 \pm 2{\cdot}9$, $7{\cdot}2 \pm 2{\cdot}6$ and $8{\cdot}6 \pm 3{\cdot}9$ ms at −80, −70 and −60 mV, respectively; mean HW was 29 ± 18, 43 ± 25 and 59 ± 23 ms at −80, −70 and −60 mV, respectively).

In Fig. 7*C* we demonstrate that EPSP broadening at increasing stimulus intensity (upper-left traces) was caused by the NMDA EPSP slowing down (lower-left traces). This change in the NMDA EPSP was similar to that produced by a change in holding membrane potential while maintaining the EPSP amplitude constant (upper- and lower-right traces). Therefore, as well as enhancing NMDA EPSP amplitude (see Fig. 5), membrane depolarization induces the NMDA component to slow down along the potential trajectory of the EPSP. This result shows that the state of NMDA channel activation is determined by the absolute depolarization produced by the EPSP. It turns out that the strong activation occurring from the holding potential of −70 mV in Fig. 7*A* and *B* reflects the state of NMDA channels at around −55 mV, which is indeed the potential at which inward NMDA currents in granule cells reach their maximum amplitude (D'Angelo *et al.* 1994*b*).

These dynamic changes in the NMDA EPSP, together with fast inward rectification, explain the quasi-linear EPSP summation and EPSP broadening during mossy fibre recruitment (Table 1).

Repetitive mossy fibre synapse activation

Repetitive activity is the physiological mode of mossy fibre discharge *in vivo* (Eccles *et al.* 1967; Ito, 1984). To reproduce this condition, trains of stimuli of intensities sufficient to activate two synapses and lasting 200–500 ms were applied at the frequencies of 10, 20, 50 and 100 Hz from holding potentials of −60, −70 and −80 mV (Fig. 8*A*). Activation of stimulus trains was delayed until post-tetanic EPSP potentiation developing at the highest frequencies (50–100 Hz) had subsided (1–2 min). In order to prevent long-term changes in synaptic efficacy (Collingridge *et al.* 1988*b*; Collingridge, 1992), trains at the highest frequencies were kept short (<200 ms) and were not repeated more than 2–4 times in the same trial. In fact, single EPSPs recorded before and after each train set (Fig. 8*B*) remained stable in eight out of eleven cells, whereas in the remaining three cells amplitude was potentiated (not shown). The nature of EPSP amplitude potentiation was not further investigated.

Two effects were evident during repetitive mossy fibre stimulation (Fig. 8*A*, top traces): EPSP summation and action potential firing were enhanced both by increasing the stimulus frequency and making the holding membrane potential less negative. Pharmacological block of the NMDA receptors (Fig. 8*B*) markedly reduced both EPSP summation and action potential firing (Fig. 8*A*, bottom traces).

EPSP summation during trains

As shown in Fig. 9*A*, the dynamics of EPSP temporal summation was investigated by measuring membrane potential at the peak (filled circles) and the base (filled squares) of individual EPSPs. Both the peak and base of the EPSP increased during the train, while their difference, which is the amplitude of individual EPSPs, decreased (filled triangles). Two opposing processes, temporal summation and EPSP amplitude depression, therefore

determined the extent of membrane depolarization during high-frequency synaptic transmission. Both temporal summation and EPSP amplitude depression increased the higher the input frequency, with a threshold at about 10 Hz (Fig. 9*B*, symbols as above).

Blocking the NMDA receptors caused a substantial reduction in base depolarization, while amplitudes of individual EPSPs and EPSP depression were much less affected (Fig. 9*A* and *B*, open symbols). It turns out that temporal summation was mainly determined by the NMDA component, while amplitude depression mainly affected the non-NMDA component of the EPSPs.

The NMDA component showed a considerable increase during the train (Fig. 9*A*, crosses). At the base of the fourth EPSP, the NMDA component was about 6 times as large at 100 Hz than at 20 Hz input frequency (Fig. 9*B*, crosses). Similar results were observed in all the eight cells covered in the analysis.

The process of NMDA EPSP summation was further investigated. In Fig. 9*C*, the NMDA component in a

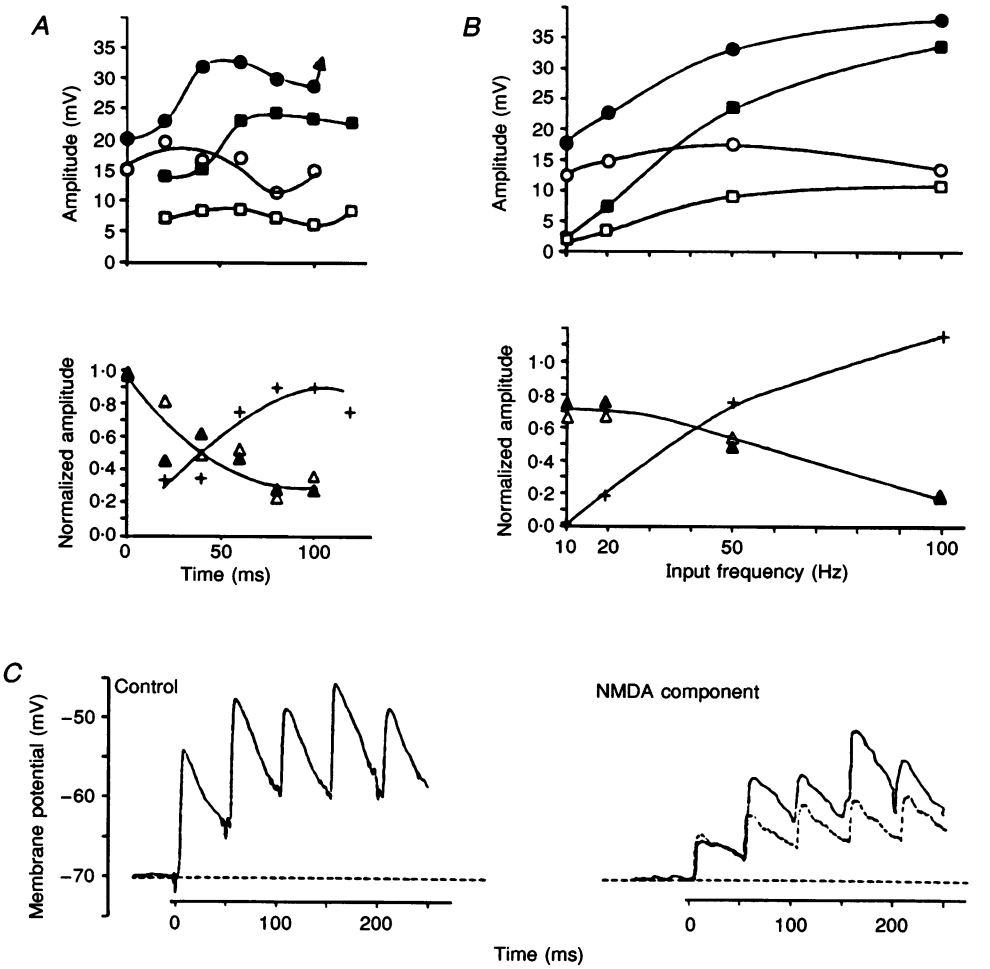

Figure 9. EPSP summation during high-frequency stimulation

A, time course of EPSP summation during a 50 Hz train (holding potential = −80 mV). Data were obtained by averaging 4 traces in the same cell. The top panel shows depolarization during the train measured at the peak (circles) and at the base of each EPSP (squares). The upward arrow indicates action potential activation. The bottom panel gives amplitudes of individual EPSPs (triangles) and of the NMDA component (crosses) normalized by the mean EPSP amplitude before the train. The NMDA component was measured at the base of individual EPSPs by subtracting non-NMDA from control EPSPs. Both in top and bottom panels, filled symbols indicate control conditions and open symbols, the application of 100 μM APV + 50 μM 7-Cl-Kyn. *B*, EPSP summation and depression at different frequencies measured at the fourth EPSP in the trains (same cell and symbols as in *A*). *C*, the NMDA component in a 20 Hz train (holding potential = −70 mV). Left, control train; right, NMDA component. The dashed line is the simulated trace obtained from summing 4 identical NMDA EPSPs measured at low-frequency delayed by 50 ms one from each other.

20 Hz train (right, solid line) is compared with the sum of individual NMDA EPSPs shifted by 50 ms one from each other (right, dashed line). This artificial trace simulates NMDA EPSP summation irrespective of whether or not membrane depolarization develops in the parent train (left). The experimental NMDA component in EPSPs next to the first one was about twice as large as the simulated one, suggesting that the increase and slowdown of the NMDA component during membrane depolarization demonstrated at low frequency (cf. Fig. 7) brought about a significant enhancement in EPSP temporal summation in high-frequency trains.

Input–output relationship in granule cells

The input–output relationship in a cerebellar granule cell in control conditions and after block of NMDA receptors is shown in Fig. 10*A* and similar plots were obtained from seven other cells. Making the holding membrane potential less negative shifted the input–output curves to the left and usually steepened them. At an input frequency of 50 Hz, mean output frequency was 25·5 ± 8·2, 13·1 ± 6 and 9·6 ± 8·5 Hz at −60, −70 and −80 mV, respectively ($n = 8$). NMDA receptor block greatly reduced the probability of spike firing, shifting the input–output curves to the right and reducing their steepness (Fig. 10*B*). At an input frequency of 50 Hz, mean output frequency after NMDA receptor block was 2·8 ± 5·5, 0 and 0 Hz at −60, −70 and −80 mV, respectively ($n = 8$).

DISCUSSION

In this paper we investigated the excitatory action of mossy fibres on individual granule cells of the rat cerebellum in a slice preparation using current-clamp recordings in the whole-cell configuration of patch-clamp. Although the whole-cell technique has been applied to investigate synaptic and voltage-dependent currents, knowledge of functional granule cell properties has relied to date on morphological evidence and extracellular recordings *in vivo* (Eccles *et al.* 1967; Ito, 1984). The analysis of EPSP pharmacology, amplitude and time course revealed that voltage dependence of the NMDA component and membrane inward rectification determine a marked voltage dependence in EPSPs. The main finding is the prominent role of NMDA receptor activation in determining both EPSP properties and granule cell coding of high-frequency mossy fibre activity.

Since recordings were performed beyond 21 days after birth, when migration and major developmental changes of membrane and synaptic properties have been completed (Garthwaite & Brodbelt, 1989; D'Angelo *et al.* 1993; D'Angelo, Rossi, De Filippi, Magistretti & Taglietti, 1994*a*; Farrant, Feldmeyer, Takahashi & Cull-Candy, 1994), the present results relate to granule cells at a mature stage of development.

Subthreshold and firing properties of granule cells

Rat cerebellar granule cells showed pronounced inward rectification in the subthreshold range reflecting a true increase of input resistance (Wilson, 1992) rather than activation of slow inward currents. This is in agreement with the absence of sizeable Ca^{2+} or Na^{+} currents at potentials lower than about −50 mV (Rossi *et al.* 1994; D'Angelo *et al.* 1994*a*). These currents might generate inward rectification together with a reduction of input resistance. Unlike turtle cerebellar granule cells (Gabbiani, Midtgaard & Knoepfel, 1994), no 'sag' in the hyperpolarizing direction or rebound depolarization/hyperpolarization was observed (cf. Fig. 2*A*). Granule cell inward rectification in the rat therefore seems to be different from that in turtle cerebellum.

Action potentials in rat cerebellar granule cells were made up of a fast sodium spike followed by deep after-hyperpolarization. The granule cells were not autorhythmic and fired repeatedly with little or no adaptation when

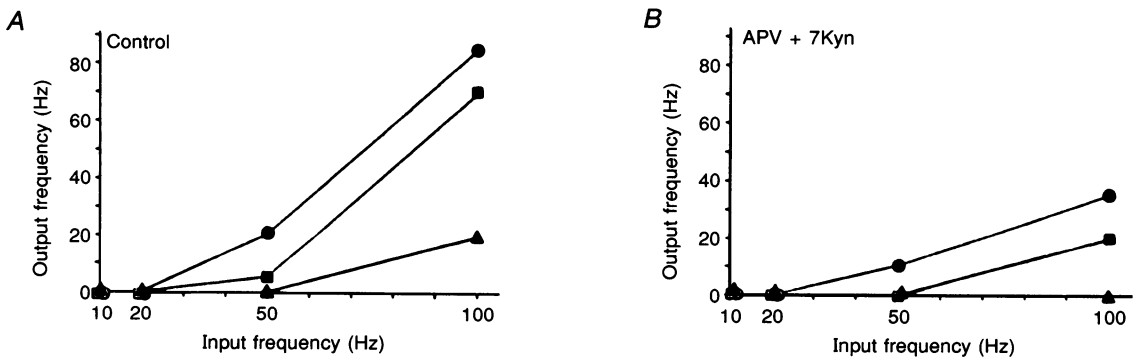

Figure 10. Input–output relationship for action potential firing during repetitive stimulation

Data are obtained from a granule cell before (left) and after (right) applying 100 μM APV + 50 μM 7-Cl-Kyn. The *x*-axis shows stimulation frequency and the *y*-axis firing frequency of the neuron. Holding potential was either −80 (▲), −70 (■) or −60 mV (●).

stimulated with current injection. The firing properties of granule cells – high attainable frequencies, low adaptation and nearly linear frequency coding of injected current – resemble those of fast spiking interneurons in the cerebral cortex (Connors & Gutnick, 1990), and would enable granule cells to translate incoming mossy fibre volleys into a related pattern of high-frequency activity over a wide dynamic range.

One possible drawback of the whole-cell technique is that perfusion of the cell by the pipette solution may modify sensitive intracellular mechanisms and the electrical response. It should be noted, however, that no intrinsic spike activity was detected before rupturing the patch (see for instance Llano & Gershenfeld, 1993) and that the basic electrophysiological properties reported here were similar when unwanted changes of cytoplasmic composition were prevented by using the perforated-patch technique (unpublished). Similar resting membrane potential (−62 *vs.* −58 mV) and firing properties were also observed in granule cells of the turtle cerebellum recorded by means of conventional microelectrode techniques (Gabbiani *et al.* 1994).

The mossy fibre–granule cell relay in a slice preparation

EPSP activation was achieved by stimulating either the mossy fibre bundle or the edge of the molecular layer, in the latter case eliciting a sort of mossy fibre 'axon reflex' resembling that obtained by 'LOC' and transfolial stimulation *in vivo* (Eccles *et al.* 1967). Antidromic stimulation could also elicit action potentials back-propagating along the granule cell axon.

As expected from the organization of the mossy fibre–granule cell relay, EPSPs were built up by activating up to five independent mossy fibres (Ito, 1984). Simultaneous activity in more than one or two mossy fibres was usually needed to induce one or a few granule cell action potentials. This finding, together with the observation that simultaneous activity in about fifty granule cells is needed to activate a Purkinje cell (Barbour, 1993), indicates a numerical transfer of 100–150 mossy fibres (Purkinje cell)$^{-1}$. The effectiveness of the mossy fibre pathway may be slightly different *in vivo* depending on the higher temperature and on the presence of Golgi neuron inhibition (Midtgaard, 1992). However, we note that in extracellular recordings from putative individual granule cells *in vivo*, the EPSP exhibited quite a large all-or-nothing component before being endorsed by one or a few spikes at a higher stimulus intensity (cf. Fig. 77 in Eccles *et al.* 1967), supporting the view that more than one synapse is needed both *in vivo* and *in vitro* to activate a granule cell.

In the present recordings, granule cell action potentials were activated within 4 ms at 30 °C, a latency similar to the N_2 wave latency measured at the same temperature in cerebellar slices (Garthwaite & Brodbelt, 1989), but longer than the 2–3 ms measured at 37 °C *in vivo*. The longer latencies of mossy fibre-activated action potentials, as well as the slower apparent conduction velocity along the granule cell axon (0·2 *vs.* 0·3 m s^{-1}), may be due to the fact that the temperature maintained in the slice was lower than that in the *in vivo* preparations.

EPSP amplitude

Unitary granule cell EPSPs (11·4 ± 2·1 mV) were 5 to 100 times larger in size than EPSPs generated in hippocampal, neocortical and spinal cord neurons (100 μV to 2 mV: see Redman, 1990; Miles, Wong & Traub, 1991). Two structural factors related to the small neuronal size helped to generate large EPSPs in granule cells, whose synaptic currents (Silver *et al.* 1992; D'Angelo *et al.* 1993) are in the same amplitude range as in other neurons (e.g. Stern, Edwards & Sakmann, 1992). First, granule cell input resistance is relatively higher than in other central neurons (cf. Spruston *et al.* 1994), causing greater depolarization following synaptic current injection. Secondly, as suggested by the present results and mathematical modelling (Silver *et al.* 1992; D'Angelo *et al.* 1993; Rossi *et al.* 1994; Gabbiani *et al.* 1994), electrotonic attenuation of EPSP transmission from synapses to soma is likely to be much smaller in granule cells than in greater neurons (Spruston *et al.* 1994). Moreover, voltage-dependent activation of the NMDA conductance enhances membrane depolarization while inward rectification, by increasing membrane resistance, acts to counterbalance decreasing driving force and loss of electrotonic compactness during depolarization (Wilson, 1992). These factors, by enhancing membrane depolarization and voltage transmission from synapses to soma, favour excitability, compensating for the small number of mossy fibres impinging on a granule cell.

As proposed at other central synapses, little variability of granule cell EPSP amplitude at a given stimulus intensity may reflect little variability in the quantum content and/or in the quantum size (Redman, 1990). EPSP quantal properties were not investigated in the present study.

EPSP voltage dependence: the role of NMDA receptors

Granule cell EPSPs were brought about by non-NMDA and NMDA receptor activation. Although non-NMDA receptors caused the bulk of EPSP amplitude, the contribution of NMDA receptors was substantial (30% at the holding potential of −70 mV). Moreover, NMDA receptors controlled EPSP kinetics and were principally responsible for two voltage-dependent properties of granule cell EPSPs. First, EPSPs showed a transient increase as they crossed potentials around −60 mV, due to a voltage-dependent increase in the NMDA component, reflecting the removal of Mg^{2+} block from the NMDA channel (Asher & Nowak, 1988). Secondly,

granule cell EPSPs showed a marked slowdown in rising and decay kinetics at depolarized membrane potentials, caused by a slowdown in the NMDA component (Keller, Konnerth & Yaari, 1991). Both EPSP properties are consistent with voltage-clamp analysis of NMDA synaptic conductance in cerebellar granule cells (D'Angelo *et al.* 1994*b*). Activation of the NMDA conductance at rather negative membrane potentials may reflect reduced block by Mg^{2+} as described for recombinant receptors containing the NR2C NMDA-receptor subunit (Monyer *et al.* 1992). NMDA receptors with NR2C-like properties are expressed in mature cerebellar granule cells (Farrant *et al.* 1994).

The prominent role of the NMDA component in determining EPSP amplitude and kinetics can be better understood if we consider that it occurred at low-frequency stimulation and in the presence of a physiological Mg^{2+} concentration. In comparable conditions a major contribution by the NMDA component has also been reported in hippocampal granule cells (Lambert & Jones, 1990), whereas in hippocampal (Collingridge *et al.* 1988*a*) and neocortical pyramidal neurons (Sutor & Hablitz, 1989) the NMDA component did not contribute substantially to low-frequency synaptic transmission near rest. It seems likely that the different contribution of the NMDA component to synaptic transmission arises from differences at NMDA conductance level and/or different NMDA to non-NMDA receptor proportions. In fact, the NMDA conductance kinetics were voltage dependent both in cerebellar (D'Angelo *et al.* 1994*b*) and hippocampal granule cells (Keller *et al.* 1991), but not in hippocampal pyramidal neurons (Hestrin, Nicoll, Perkel & Sah, 1990). Different NMDA conductances and consequently EPSP properties, may depend on the region-specific expression of NMDA receptor subunits (Monaghan and Anderson, 1991; Monyer *et al.* 1992) and may be relevant to the function subserved by NMDA receptors in a given neuronal circuit.

EPSP summation and depression during high frequency mossy fibre activity

During high-frequency synaptic transmission, granule cell depolarization was sustained by a positive balance of temporal summation *vs.* EPSP amplitude depression. Interestingly, NMDA receptors gained control of depolarization along the trains, due to the simultaneous increase in the NMDA and decrease in the non-NMDA component.

The enhancement of the NMDA component at high-frequency stimulation was presumably determined by a voltage-dependent increase and slowdown of the NMDA component during membrane depolarization, although we cannot rule out additional mechanisms, like glutamate spill-over and activation of extrasynaptic NMDA receptors (Lambert & Jones, 1990). On the other hand, desensitization caused by transient accumulation of synaptic glutamate might favour the selective decrease of the non-NMDA component (Trussel, Zhang & Raman, 1993), as desensitization of the NMDA receptors is prevented by extracellular glycine (Mayer *et al.* 1989; Thomson, 1989). It should be noted that depressed glutamate release would reduce activation of both non-NMDA and NMDA synaptic receptors.

High-frequency activation of the NMDA component in cerebellar granule cells occurred at more negative membrane potentials and frequency dependence was 3-fold steeper than in hippocampal pyramidal cells (Collingridge *et al.* 1988*b*), but this lower performance of the NMDA system in pyramidal neurons might be partly caused by the presence of inhibitory activity.

Coding of high-frequency mossy fibre activity

High-frequency stimulation (20–100 Hz) induced a repetitive discharge of action potentials similar to that evoked upon steady current injection at the granule cell soma. Our findings on EPSP summation and voltage dependence suggest that output frequency was mainly determined by the depolarizing effect of sustained NMDA receptor activation, since the NMDA relative to non-NMDA contribution was also conspicuous at the negative membrane potentials visited during spike after-hyperpolarization. Indeed, the block of NMDA receptors caused a dramatic reduction of the output frequency. In particular, synaptic integration was nearly abolished at input frequencies $\leqslant 50$ Hz, where output frequency decreased by $>90\%$. This finding appears to be of significance, since any modulation in the state of granule cell NMDA receptors would fine tune the efficacy of incoming mossy fibre volleys in the physiological frequency range (<200 Hz; Kase, Miller & Noda, 1980).

Conclusions

The present investigation extends previous knowledge of the mossy fibre–granule cell relay function (Eccles *et al.* 1967; Ito, 1984) at the intracellular level, suggesting a crucial role for NMDA receptor activation in determining granule cell information transfer to the cerebellar cortex. The wide unitary EPSP amplitude, which is primarily determined by a high input resistance and compact electrotonic structure, is further enhanced by inward rectification and voltage-dependent increase in the NMDA EPSP component, enabling granule cells to fire action potentials following synchronous activity in just two to three mossy fibres synapses. It is suggested that the marked voltage dependence of the EPSP time course, which was mainly caused by voltage dependence in NMDA conductance, promotes the NMDA receptor-dependent enhancement of granule cell coding observed during repetitive mossy fibre activity. The functional implications of these findings may depend critically on inhibitory activity in the Golgi cell–granule cell loop (cf. Fig. 87 in Eccles *et al.* 1967), which may modulate the voltage-dependent activation in NMDA conductance.

Finally, NMDA receptor activation may be relevant to the induction of long-term changes in synaptic efficacy (Collingridge, 1992).

ASHER, P. & NOWAK, L. (1988). The role of divalent cations in the *N*-methyl-D-aspartate responses of mouse central neurones in culture. *Journal of Physiology* **399**, 247–266.

BARBOUR, B. (1993). Synaptic currents evoked in Purkinje cells by stimulating individual granule cells. *Neuron* **11**, 759–769.

BARDONI, R. & BELLUZZI, O. (1993). Kinetic study and numerical reconstruction of A-type current in granule cells of rat cerebellar slices. *Journal of Neurophysiology* **69**, 2222–2231.

COLLINGRIDGE, G. L. (1992). The mechanism of induction of NMDA receptor-dependent long-term potentiation in the hippocampus. *Experimental Physiology* **77**, 771–797.

COLLINGRIDGE, G. L., HERRON, C. E. & LESTER, R. A. J. (1988*a*). Synaptic activation of *N*-methyl-D-aspartate receptors in the Schaffer collateral–commissural pathway of rat hippocampus. *Journal of Physiology* **399**, 283–300.

COLLINGRIDGE, G. L., HERRON, C. E. & LESTER, R. A. J. (1988*b*). Frequency-dependent *N*-methyl-D-aspartate receptor-mediated synaptic transmission in rat hippocampus. *Journal of Physiology* **399**, 301–312.

CONNORS, B. W. & GUTNICK, M. J. (1990). Intrinsic firing patterns of diverse neocortical neurons. *Trends in Neurosciences* **13**, 99–104.

CULL-CANDY, S. G., MARSHALL, C. G. & OGDEN, D. (1989). Voltage-activated membrane currents in rat cerebellar granule neurones. *Journal of Physiology* **414**, 179–199.

D'ANGELO, E., ROSSI, P., DE FILIPPI, G., MAGISTRETTI, J. & TAGLIETTI, V. (1994*a*). The relationship between synaptogenesis and expression of voltage-dependent currents in cerebellar granule cells *in situ*. *Journal de Physiologie* **88**, 197–207.

D'ANGELO, E., ROSSI, P. & GARTHWAITE, J. (1990). Dual-component NMDA receptor currents at a single central synapse. *Nature* **346**, 467–470.

D'ANGELO, E., ROSSI, P. & TAGLIETTI, V. (1993*a*). Different proportions of N-methyl-D-aspartate and non-N-methyl-D-aspartate receptor currents at the mossy fibre-granule cell synapse of developing rat cerebellum. *Neuroscience* **53**, 121–130.

D'ANGELO, E., ROSSI, P. & TAGLIETTI, V. (1994*b*). Voltage-dependent kinetics of N-methyl-D-aspartate synaptic currents in rat cerebellar granule cells. *European Journal of Neuroscience* **6**, 640–645.

ECCLES, J. C., ITO, M. & SZENTAGOTHAI, J. (1967). *The Cerebellum as a Neuronal Machine*. Springer Verlag, Berlin.

EDWARDS, F. A., KONNERTH, A., SAKMANN, B. & TAKAHASHI, T. (1989). A thin slice preparation for patch-clamp recordings from neurones of the mammalian central nervous system. *Pflügers Archiv* **414**, 600–612.

FARRANT, M., FELDMEYER, D., TAKAHASHI, T. & CULL-CANDY, S. G. (1994). NMDA-receptor channel diversity in the developing cerebellum. *Nature* **368**, 335–339.

FORSYTHE, I. D. & WESTBROOK, G. L. (1988). Slow excitatory postsynaptic currents mediated by *N*-methyl-D-aspartate receptors on cultured mouse central neurones. *Journal of Physiology* **396**, 515–533.

GABBIANI, F., MIDTGAARD, J. & KNOEPFEL, T. (1994). Synaptic integration in a model of cerebellar granule cells. *Journal of Neurophysiology* **72**, 999–1009.

GARTHWAITE, J. & BRODBELT, A. R. (1989). Synaptic activation of N-methyl-D-aspartate and non-N-methyl-D-aspartate receptors in the mossy fibre pathway in adult and immature rat cerebellar slices. *Neuroscience* **29**, 401–412.

HENDERSON, G., JOHNSON, J. W. & ASHER, P. (1990). Competitive antagonists and partial agonists at the glycine modulatory site of the mouse *N*-methyl-D-aspartate receptor. *Journal of Physiology* **430**, 189–212.

HESTRIN, S., NICOLL, R. A., PERKEL, D. J. & SAH, P. (1990). Analysis of excitatory synaptic action in pyramidal cells using whole-cell recording from rat hippocampal slices. *Journal of Physiology* **422**, 203–225.

ITO, M. (1984). *The Cerebellum and Neuronal Control*, pp. 44–93, Raven Press, New York.

KASE, M., MILLER, D. C. & NODA, H. (1980). Discharges of Purkinje cells and mossy fibres in the cerebellar vermis of the monkey during saccadic eye movements and fixation. *Journal of Physiology* **300**, 539–555.

KELLER, B. U., KONNERTH, A. & YAARI, Y. (1991). Patch clamp analysis of excitatory synaptic currents in granule cells of rat hippocampus. *Journal of Physiology* **435**, 275–293.

LAMBERT, J. D. C. & JONES, R. S. G. (1990). A reevaluation of excitatory amino acid-mediated synaptic transmission in rat dentate gyrus. *Journal of Neurophysiology* **64**, 119–132.

LLANO, I. & GERSCHENFELD, H. M. (1993). Inhibitory synaptic currents in stellate cells of rat cerebellar slices. *Journal of Physiology* **468**, 177–200.

MAYER, M. L., VYKLICKY, L. JR & CLEMENTS, J. (1989). Regulation of NMDA receptor desensitization in mouse hippocampal neurons by glycine. *Nature* **338**, 425–427.

MIDTGAARD, J. (1992). Membrane properties and synaptic responses of Golgi cells and stellate cells in the turtle cerebellum *in vitro*. *Journal of Physiology* **457**, 329–354.

MILES, R., WONG, R. K. S. & TRAUB, R. D. (1991). Recurrent excitatory synapses between CA3 neurons in the hippocampus. In *Excitatory Amino Acids and Synaptic Transmission*, ed. WHEAL, H. V. & THOMSON, A. M., pp. 141–154. Academic Press, London.

MONAGHAN, D. T. & ANDERSON, K. J. (1991). Heterogeneity and organization of excitatory amino acid receptors and transporters. In *Excitatory Amino Acids and Synaptic Transmission*, ed. WHEAL, H. V. & THOMSON, A. M., pp. 33–54. Academic Press, London.

MONYER, H., SPRENGEL, R., SHOEPFER, R., HERB, A., HIGUCHI, M., LOMELI, H., BURNASHEV, N., SAKMANN, B. & SEEBURG, P. H. (1992). Heteromeric NMDA receptors: molecular and functional distinction of subtypes. *Science* **256**, 1217–1221.

MUGNAINI, E., ATLURI, R. L. & HOUK, J. C. (1974). Fine structure of granular layer in turtle cerebellum with emphasis on large glomeruli. *Journal of Neurophysiology* **37**, 1–29.

REDMAN, S. (1990). Quantal analysis of synaptic potentials in neurons of the central nervous system. *Physiological Reviews* **70**, 165–198.

ROSSI, P., D'ANGELO, E., MAGISTRETTI, J., TOSELLI, M. & TAGLIETTI, V. (1994). Age-dependent expression of high-voltage activated calcium currents during cerebellar granule cell development *in situ*. *Pflügers Archiv* **429**, 107–116.

SILVER, R. A., TRAYNELIS, S. F. & CULL-CANDY, S. G. (1992). Rapid-time-course miniature and evoked excitatory currents at cerebellar synapses *in situ*. *Nature* **355**, 163–166.

SPRUSTON, N., JAFFE, D. B. & JOHNSTON, D. (1994). Dendritic attenuation of synaptic potentials and currents: the role of passive membrane properties. *Trends in Neurosciences* **17**, 161–166.

STERN, P., EDWARDS, F. A. & SAKMANN, B. (1992). Fast and slow components of unitary EPSCs on stellate cells elicited by focal stimulation in slices of rat visual cortex. *Journal of Physiology* **449**, 247–278.

SUTOR, B. & HABLITZ, J. J. (1989). EPSPs in rat neocortical neurons *in vitro*. II. Involvement of N-methyl-D-aspartate in the generation of EPSPs. *Journal of Neurophysiology* **61**, 621–634.

THOMSON, A. M. (1989). Glycine modulation of the NMDA receptor/channel complex. *Trends in Neurosciences* **12**, 349–353.

TRUSSEL, L. O., ZHANG, S. & RAMAN, I. M. (1993). Desensitization of AMPA receptors upon multiquantal neurotransmitter release. *Neuron* **10**, 1185–1196.

WILSON, C. J. (1992). Dendritic morphology, inward rectification and the functional properties of neocortical neurons. In *Single Neuron Computation*, ed. MCKENNA, T., DAVIS, J. & ZORNETZER, S. F., pp. 141–172. Academic Press, San Diego, CA, USA.

Acknowledgements

This work was supported by grants from the Ministero della Ricerca Scientifica e Tecnologica and Consorzio Interuniversitario Nazionale di Fisica della Materia. P. R. was supported by a grant from Crinos S.p.A., Villa Guardia (Como).

Received 20 June 1994; accepted 10 September 1994.